NUCLEAR ORIENTATION STUDIES OF LOCAL MOMENTS IN NOBLE METAL HOSTS

R. J. Holliday and W. Weyhmann

Solid State and Low Temperature Physics Group

SCHOOL OF PHYSICS AND ASTRONOMY

September, 1970
UNIVERSITY OF MINNESOTA
MINNEAPOLIS, MINNESOTA

Work supported in part by the U.S. Atomic Energy Commission

DISCLAIMER

COO-1569-67

NUCLEAR ORIENTATION STUDIES OF LOCAL MOMENTS IN NOBLE METAL HOSTS*

R. J. Holliday and W. Weyhmann

Tate Laboratory of Physics

University of Minnesota, Minneapolis, Minnesota

*Work supported in part by the U. S. Atomic Energy Commission under Contract No. AT(11-1) 1569.

ABSTRACT

The internal magnetic fields at Co nuclei as a very dilute impurity in Au, Cu, and a series of Au-Cu alloys were determined by low temperature nuclear orientation of ^{60}Co. ^{54}Mn in Cu was used as the thermometer. A straight line fitted to all the data gives:

$$H_{int}(kG) = (3.2\pm3.5)+(1.29\pm0.11)H_{app}(kG) \quad \text{(Au)}$$

$$H_{int} = (-2.6\pm2.8)+(1.28\pm0.08)H_{app} \quad \text{(AuCu)}$$

$$H_{int} = (5.7\pm3.9)+(0.92\pm0.12)H_{app} \quad \text{(Cu)}$$

If the intercept of the straight lines fit only to the high H_{app} points is forced to go through zero, the value of H_{int}/H_{app} varies smoothly as the host changes from Au to Cu through a series of Au-Cu alloys.

Contents

List of Figures

I. INTRODUCTION

In studying local moments, the first question one must ask is whether or not a local moment exists. That is, given a single transition metal impurity in an otherwise nonmagnetic metal, what are the conditions under which the impurity will be "magnetic"? This thesis will attempt to answer the above question for cobalt as a dilute impurity in various noble metal hosts. The term "magnetic" and "nonmagnetic" will be used in a comparative sense to describe whether or not the Knight shift exceeds 5-10%.

Cobalt is on the border of the transition from magnetic to nonmagnetic behavior. It is in this region that much work needs to be done as theoretical methods tend to break down for marginal behavior. Also by studying systems of this type it might be possible to determine more explicitly the conditions necessary for local moment formation. Cr, Mn, and Fe are known to show Kondo behavior in Cu and Au hosts.[1] Experiments have been performed on these with the impurity level below 100 ppm. For Co and V, the experiments have required concentrations above 0.1% because of the low impurity susceptibility. As the concentration is raised above 1%, the magnetic moment per atom increases for Co impurities and the

Knight shift changes from negative to positive for V impurities. It has been concluded that in the low concentration limit, V and Co will be nonmagnetic.[2,3,4] This thesis presents the first measurements of the hyperfine interaction of Co in Au, Cu, and Au-Cu alloys at very low concentrations and temperatures.

The experimental technique used was low temperature nuclear orientation. Nuclear orientation is a particularly useful technique for the study of Co as an impurity, as very low concentrations can be used. The temperature is limited to the region below 0.050 K, which should be in the T=0 limit for Co impurities.

II. THEORY

A. Nuclear Orientation

The theory of nuclear orientation has been discussed completely elsewhere.[5,6,7,8] Only a brief outline emphasizing low-temperature, thermal equilibrium orientation in metals is given here.

If a magnetic field, H, is applied to a nucleus of total angular momentum (spin), I, the degeneracy of the 2I+1 nuclear magnetic substates (hyperfine levels) is lifted. Each substate now has a different orientation with respect to the applied field. The substates are separated equally in energy with

$$\Delta E = \mu H/I.$$

At room temperature these levels are equally populated by the nuclei. In such a system the nuclei are randomly oriented. However, if by some means, a distribution is achieved so that the levels are not uniformly populated, the system of nuclei is said to be oriented.

If there are several energy states available to a system in thermodynamic equilibrium, the states will be populated in proportion to the Boltzmann factor and the relative population of the substates will be

$$W(m) = e^{-m\beta} / \sum_m e^{-m\beta}$$

where m is the quantum number denoting the projection of the substates on the axis given by the direction of the magnetic field so that $-I \leq m \leq I$ and $\beta = \mu H/IkT$. H is the magnetic field at the nucleus and μ is the nuclear magnetic moment, thus the m states with the lowest energy will be preferentially populated.

To achieve orientation β must be made as large as possible which implies, for reasonable values of μ and I, very large magnetic fields and very low temperatures.

If the oriented nuclei are radioactive, it is possible to determine the degree of orientation from the angular distribution of the emitted radiation, since the angular distribution is dependent on the populations of the magnetic substates. The angular distribution of radiation from oriented nuclei may be represented by[5]

$$W(\theta) = \sum_{k=0}^{\lambda} B_k U_k F_k P_k(\cos \theta) \qquad (1)$$

where $W(\theta)$ is defined as the number of radiations emitted by the oriented nuclei at angle θ divided by the number of radiations emitted from the nonoriented nuclei at angle θ, where θ is the angle between the direction of the applied magnetic field and the

direction of emission of the radiation. The expansion is for λ equal to 2I or 2L, whichever is smaller. Here I is the angular momentum of the nucleus before decay and L is the angular momentum carried away. For $k \geq 2I$, $B_k = 0$ and for $k \geq 2L$, $F_k = 0$.

The B_k term is the only temperature dependent coefficient in the expansion and is determined by the population distribution between the hyperfine levels of the parent nucleus. B_k is defined by the relation

$$B_k = (2k+1)^{\frac{1}{2}} \sum_m C(IkmO|Im)W(m),$$

where C is a Clebsch-Gordon coefficient. B_1, B_2, and B_4 have been tabulated as functions of the Boltzmann factor by Blin-Stoyle and Grace.[5]

The U_k coefficient can best be described by use of an actual decay scheme. Fig. 1 shows the decay scheme of ^{60}Co. Although the ^{60}Co is the oriented nucleus of interest, it is much easier to observe the γ rays emitted from the excited levels of ^{60}Ni than the β particle emitted directly from the parent ^{60}Co nucleus. Therefore it is necessary to correct for the change in the magnitude and orientation of the momentum occurring during transitions preceding that observed. The U_k coefficient takes this into account. It is usually assumed, and for the cases described in this thesis it is true, that the lifetime of the intermediate

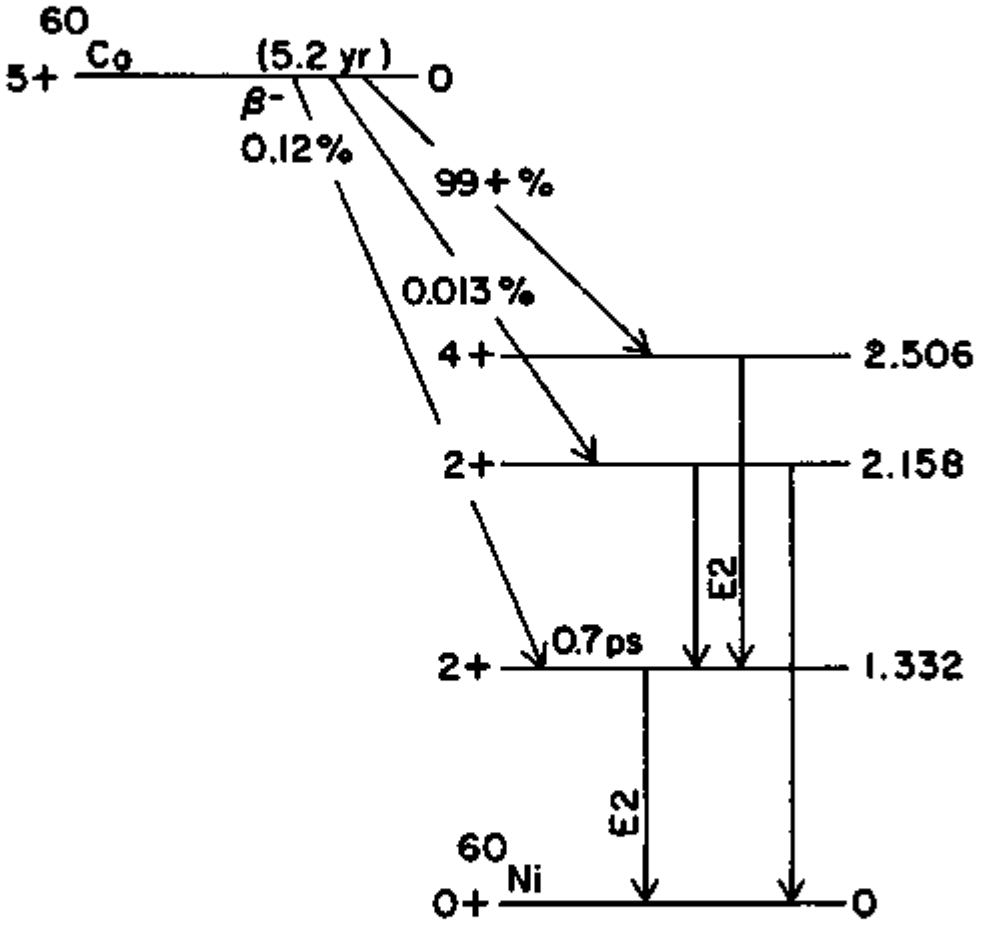

Figure 1. Decay scheme of ^{60}Co

state is so short that processes such as the interaction of the nuclear spin with the thermal vibrations of the lattice, recoil of the nucleus from its lattice position through regions of different field, changes in magnetic or electric field gradient at the nucleus due to the atomic rearrangement following a β process, or ionization or excitation of the atom do not disturb the orientation. For an unobserved transition ($I_a \xrightarrow{L} I_b$) which feeds the state from which the observed γ ray decays, the U_k is given by

$$U_k = \left[(2I_a+1)(2I_b+1)\right]^{\frac{1}{2}}(-)^{I_a+I_b-L}\, W(I_aI_aI_bI_b;kL),$$

where W is the Racah angular momentum coupling coefficient. If there is more than one unobserved transition, the final U_k is the product of those for each individual transition.

The F_k coefficient depends on the multipole character of the observed transition and upon the angular momenta of the nuclear state from which the observed transition is emitted and the final nuclear state. For an unmixed γ transition ($I_b \xrightarrow{L} I_c$), F_k is given by

$$F_k = (-)^{I_c-I_b-1}(2I_b+1)^{\frac{1}{2}}(2L+1)C(LL1-1|k0)W(I_bI_bLL;kI_c),$$

where L is the angular momentum carried away by the

γ ray. Due to the conservation of parity in γ transitions, the F_k for odd k are zero. P_k is the Legendre polynomial of order k and is the only coefficient dependent on θ. Therefore for a γ transition $W(\theta) = W(\theta+\pi)$, since $P_{k(\text{even})}$ is an even function of cos θ.

B. Local Moments[9]

1. The Friedel Model[10]

The first significant theory proposed to explain the behavior of alloys made up of transition impurity atoms in noble metals was the localized virtual-state picture presented by Friedel.[10] This theory is based on scattering theory, and strong resonance scattering of d character is assumed from the impurity potential due to a transition atom.

Friedel begins by considering an atom with a spherically symmetric potential as shown in Fig. 2a. The dashed potential is attractive enough so that it has an ℓth bound state, however the continuous curve represents a potential which is not quite strong enough to have a bound state with quantum number ℓ. The bound state has increased in energy and merged into the continuum of extended states, where it will resonate with the ℓth spherical component of the extended state with the same energy to build up two

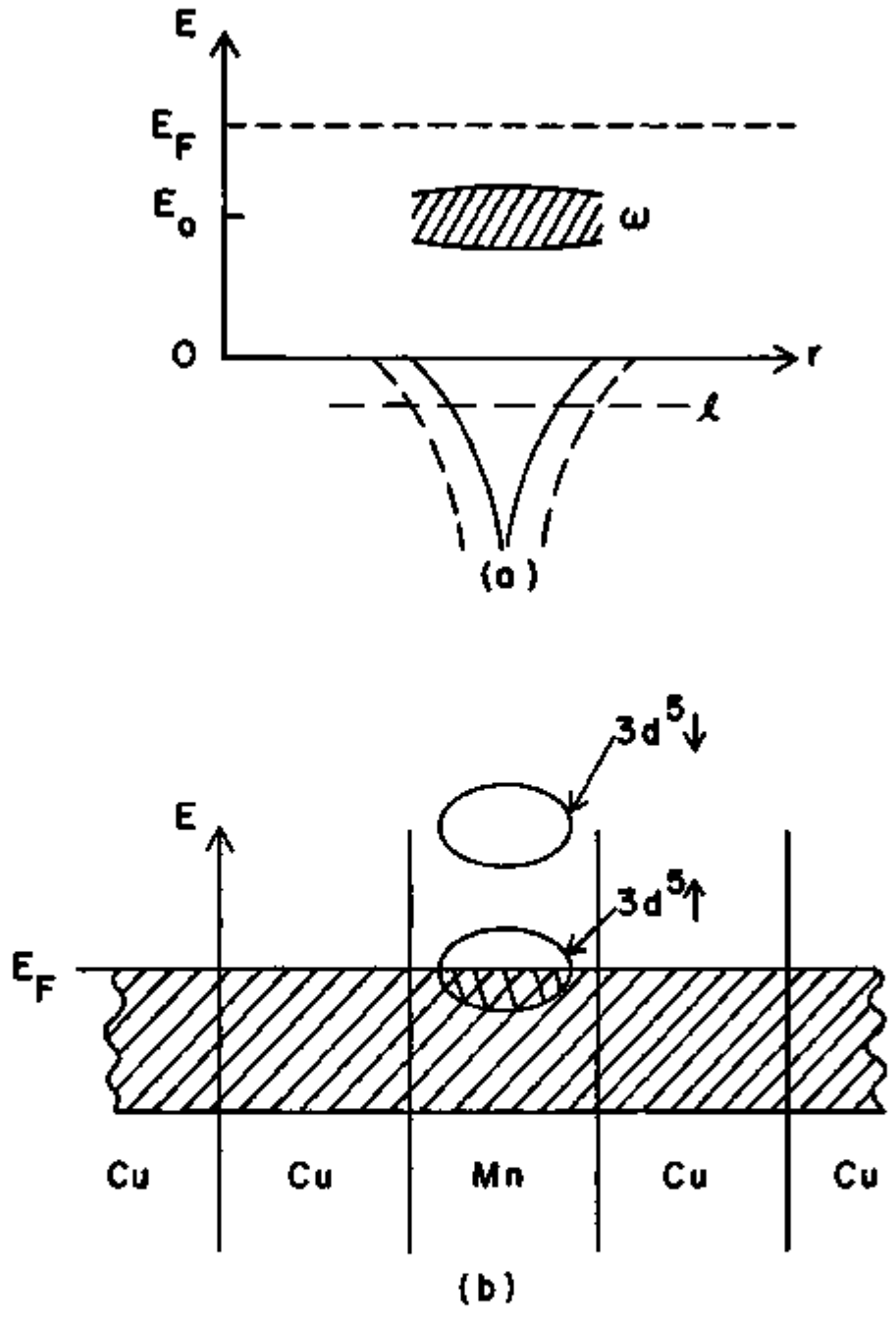

Figure 2. (a) Real bound state (dashed curves) and virtual bound state (continuous curves) in an energy versus space diagram. (b) d shell of a typical magnetic impurity split into two virtual bound levels of opposite spin directions. Taken from Ref. 10.

extended states of slightly different energies. These in turn resonate, building up a region in energy and space known as a virtual bound state which is represented by the shaded region in Fig. 2a.

The width, w, of the level increases with the amount of ℓth spherical component in the free electron state of energy E_o. Therefore w decreases for increasing ℓ and for a given ℓ it is roughly proportional to E_o (for small values of E_o). w is the order of 2 eV for $\ell = 2$ (d states) and $E_o = 7$ eV (Fermi energy of copper).

Exchange correlations tend to split the d shell into two halves of opposite spin directions. Splitting occurs if w is smaller than the energy of splitting, $p\Delta E$ per d electron. p is the number of electrons (if less than 5) or holes (otherwise) in the d shell; ΔE is the average energy gained when two d electrons with antiparallel spins are placed with their spins parallel. From atomic spectra, ΔE is 0.6 to 0.7 eV. For Cu, it is necessary that $p \geq w/\Delta E = 3$; therefore splitting should occur for impurities like Fe, Mn, and Cr but not for Ni where the number of d holes is too small. The case for Mn in Cu is shown in Fig. 2b.

2. The Anderson Model[11]

The Anderson model can best be summarized by writing the Hamiltonian:

$$H = \sum_{k,\sigma} \epsilon_k n_{k\sigma} + E(n_{d\uparrow} + n_{d\downarrow}) + U n_{d\uparrow} n_{d\downarrow} + \sum_{k,\sigma} V_{dk}(c^+_{k\sigma} c_{d\sigma} + c^+_{d\sigma} c_{k\sigma}).$$

ϵ_k is the host metal conduction electron energy for the state of momentum k; $n_{k\sigma} = c^+_k c_k$ where c^+ and c are the usual creation and destruction operators; E is the unperturbed energy of the d states of the impurity atom; U is the coulomb repulsive energy between two electrons in the same d orbital; and V_{dk} is the matrix element giving the interaction energy between d states and conduction electrons. This Hamiltonian, as written, is for a single orbital d shell state with two possible spin orientations. Anderson shows in an appendix to his paper, that this is not of major consequence.

The term which splits the spin up and spin down d orbitals is the coulomb term, U. If the unperturbed energy $E_{d\uparrow} \prec E_F$ and $E_{d\downarrow}+U \succ E_F$ then the spin up orbitals will be occupied and spin down empty, i.e., there will be a net d moment on the impurity. The effect of the mixing of the d states and free electron states, V, is to broaden the spin up and spin down levels. If this broadening is large enough to overlap the Fermi level,

then the spin up level will be partially emptied and conversely for the spin down level. See Fig. 3. This in turn causes a decrease in the coulomb energy splitting the two levels. This effect is larger the larger the density of free electrons, the larger the d to free electron admixture matrix element, V, and the smaller the energy difference between up and down states, U. If V is sufficiently large and U sufficiently small, this effect cumulates in the convergence of the spin up and spin down levels thereby causing the magnetic moment to go to zero.

Due to the difficulty caused by the particle-particle coulomb term, Anderson treats the Hamiltonian using the Hartree-Fock or self-consistent field approximation. Then by using Green's function methods, he is able to obtain the density distribution of the d state

$$\rho_{d\sigma}(\epsilon) = \Delta/\pi\left[(\epsilon - E_\sigma)^2 + \Delta^2\right],$$

where $E_\sigma = E + U\langle n_{d,-\sigma}\rangle$, and Δ is the width parameter of the virtual state given by

$$\Delta = \pi\langle V^2\rangle_{av}\,\rho(\epsilon).$$

$\rho(\epsilon)$ is the density of states for the unperturbed conduction band. Fig. 3 shows the density of states

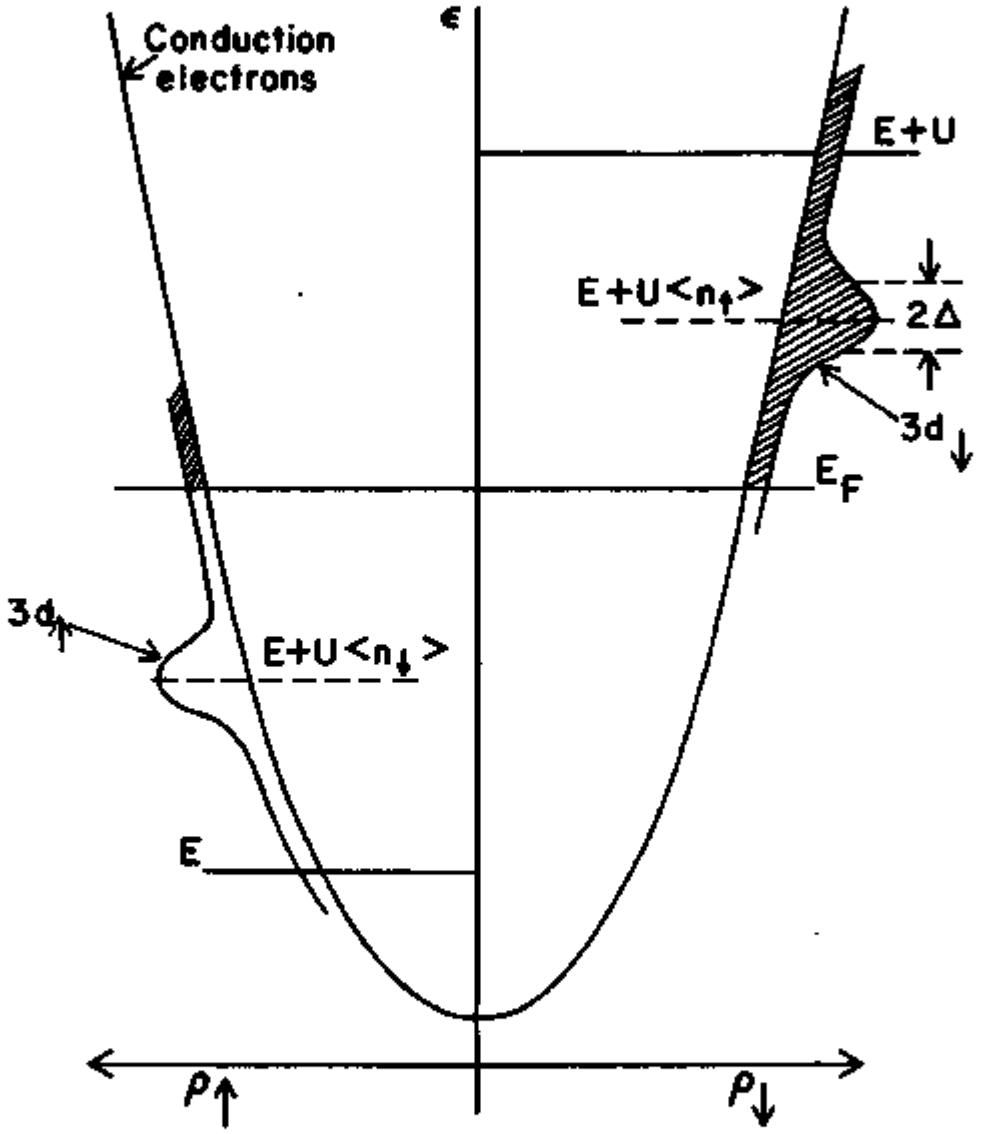

Figure 3. Density of states distributions in a magnetic case. The "humps" at $E+U\langle n_\downarrow\rangle$ and $E+U\langle n_\uparrow\rangle$ are the virtual levels of width 2Δ, for up and down spins respectively. The number of electrons $\langle n_\uparrow\rangle$ and $\langle n_\downarrow\rangle$ occupying them are to be computed from the area of the unshaded portion below the Fermi level. Taken from Ref. 11.

distribution for a typical magnetic case.

By using $\rho_{d\sigma}(\epsilon)$ to determine the total number of d electrons of spin σ, $\langle n_{d\sigma} \rangle$, and making the values of $n_{d\uparrow}$ and $n_{d\downarrow}$ self-consistent, Anderson obtains a criterion for local moment formation given by

$$\rho_d(E_F)U > 1.$$

Therefore a small density of states for the conduction band and small matrix elements for the s-d admixture make Δ small, thus favoring the appearance of the localized moment. This is thought to be the case in noble metal hosts. Also $\rho_d(E_F)$ is largest for atoms with $n_d = 5$ and decreases as one goes away from the center of the transition series. This accounts for the fact that Cr, Mn, and Fe have local moments when dissolved in noble metals.

Heeger has tried to extract values from experiment for various parameters in the Anderson model.[12] For the iron group impurities in Cu, Ag, and Au; he finds that experimental results give $U \sim 4$ eV and $\Delta = 0.4$-0.6 eV assuming a Lorentzian shape for the virtual level.

3. The Kondo Effect

A number of dilute alloys containing transition metal solutes exhibit a minimum in the electrical

resistivity versus temperature curve at low temperatures, e.g., Mn or Fe dissolved in Cu, Ag, or Au. Kondo made the first important step toward understanding this phenomenon.[13] He began by assuming that a moment existed and that it interacts with the conduction electrons by means of an interaction represented by the Hamiltonian

$$H_{s-d} = -J(r)\vec{S}\cdot\vec{s}(r),$$

where $\vec{s}$ is the conduction electron spin, $\vec{S}$ the impurity spin, and $J(r)$ is negative. This is usually simplified by assuming a point contact interaction, i.e., $H_{s-d} = -JV\vec{S}\cdot\vec{s}(0)$, where V is the atomic volume and $\vec{s}(0)$ is the conduction electron spin density at the impurity. In second quantized formalism

$$H_{s-d} = -(J/2N)\sum_{kk'}\left[S_z(c^+_{k\uparrow}c_{k'\uparrow} - c^+_{k\downarrow}c_{k'\downarrow}) + S_+c^+_{k\downarrow}c_{k'\uparrow} + S_-c^+_{k\uparrow}c_{k'\downarrow}\right].$$

Kondo found that when he carried the perturbation theory of the scattering of the conduction electrons by a single localized spin S beyond the first Born approximation, a log T term appeared in the resistivity. This logarithmic divergence with decreasing temperature indicates a breakdown of perturbation theory below a characteristic temperature given by

$$T_K = T_F \exp(-1/|J|\rho(0)),$$

where T_K is known as the Kondo temperature. T_F is the Fermi temperature, and $\rho(0)$ is the density of states per atom per spin in the host metal, evaluated at the Fermi surface.

It is thought that for $T < T_K$ the conduction electrons and impurity moment interact in such a way that a complicated many body state, also called a quasi-bound state, is formed. This state may be thought of as the high temperature localized moment surrounded by a cloud of conduction electrons with their spins polarized opposite to that of the local moment so that the net effect is to cancel the magnetic moment on the impurity. At T = 0 K, the ground state energy of the quasi-bound state should be approximately kT_K below that of the same system without the coupling.[1]

It is of considerable interest to study the effect of a magnetic field on the ground state of the above system. It is reasonable to assume that when the condition $\mu_B H = kT_K$ is satisfied, the bound state will be completely destroyed. However this has not been found experimentally to be the case.[14,15] Theoretical treatments also indicate that the bound state does not break up completely until the applied magnetic field is many times larger than the Kondo temperature.[16]

Many theoretical estimates have been made for the susceptibility of dilute impurities at low temperatures, $T \ll T_K$.[17] Heeger summarizes most of these in Table II of his review article.[12] Assuming $J < 0$, χ is found to be proportional to μ_B^2/kT_K.

Suhl and coworkers have proposed a different model based on repeated conduction electron-hole scattering in the presence of a fixed impurity potential.[18] This gives rise to fluctuations of the impurity spin. When the rate of the fluctuations is less than that of thermally produced fluctuations, the moment is well defined. However if the reverse is true, the impurity appears nonmagnetic. T_K would correspond to the point at which both rates are equal.

The measurements described in this thesis were made at such low temperatures that $T \ll T_K$ and in fact one can assume as far as comparison with theory is concerned that T = 0 K. Also such dilute alloys were used that impurity-impurity interactions can be ignored.

It is to be noted that the theoretical situation as regards local moment formation and the Kondo effect is far from complete, especially in the region of marginal local moment formation. It is in just this region, between obvious magnetic and nonmagnetic

behavior that the system, Co in noble metal hosts, studied in this thesis lies.

C. The Internal Field

The total magnetic field, H_{int}, acting at the nucleus in nonmagnetic materials may be written as

$$H_{int} = H_{app} \pm |H_{hf}| \qquad (2)$$

where H_{app} is the external, applied field and H_{hf} the hyperfine magnetic field. If H_{hf} is positive, H_{app} and H_{hf} are parallel and the positive sign in Eq. (2) is correct. If H_{hf} is negative, H_{app} and H_{hf} are antiparallel and the negative sign in Eq. (2) is correct. The hyperfine field may be written for cubic symmetry as

$$H_{hf} = (8\pi/3)g\mu_B S|\Psi(0)|^2 + g\mu_B L\langle 1/r^3\rangle$$

where the first term arises from the Fermi contact interaction.[19] $|\Psi(0)|^2$ is the unpaired s electron density at the nucleus. The second term is due to the electron orbital angular momentum, L. The orbital moment will be assumed to be quenched, i.e., L = 0.

If a large enough magnetic field is applied to a Kondo system with $T \ll T_K$, it is expected, as mentioned in the last section, that the coupling between local

moment and conduction electrons will be partially destroyed. This means that the local moment will no longer be completely cancelled. This moment will in turn affect $|\Psi(0)|^2$ and thus contribute to H_{hf}. Therefore by measuring H_{int} and from this H_{hf} by nuclear orientation, it is possible to obtain an estimate of the moment on Co atoms when dissolved as dilute impurities in various noble metal hosts.

III. EXPERIMENTAL

A. Apparatus

The basic procedure used was to cool the alloy to a low temperature by adiabatic demagnetization of a paramagnetic salt to which the alloy was thermally linked, and to apply a sufficient magnetic field to induce some orientation in the radioactive nuclei, then to measure the intensity of radiation emitted from the oriented nuclei compared with the intensity emitted from the nonoriented nuclei. The apparatus used can be divided into two separate systems: one for cooling the sample to very low temperatures in the presence of a large applied magnetic field, the other for detecting and analysing the γ radiation emitted from the sample.

1. Cooling System

This was described in detail by Smith and Weyhmann[20] and is shown schematically in Figs. 4, 5 and 6. There are two double-walled glass dewars. The outer contains liquid nitrogen and the inner liquid helium. Immersed in the liquid helium are two superconducting magnets. The magnet used for magnetizing the salt pill was made by Westinghouse and has a $2\frac{1}{2}$-inch bore and is $9\frac{1}{4}$-inch long. This magnet produces a field of 18 kG at a current of 22 amperes. The

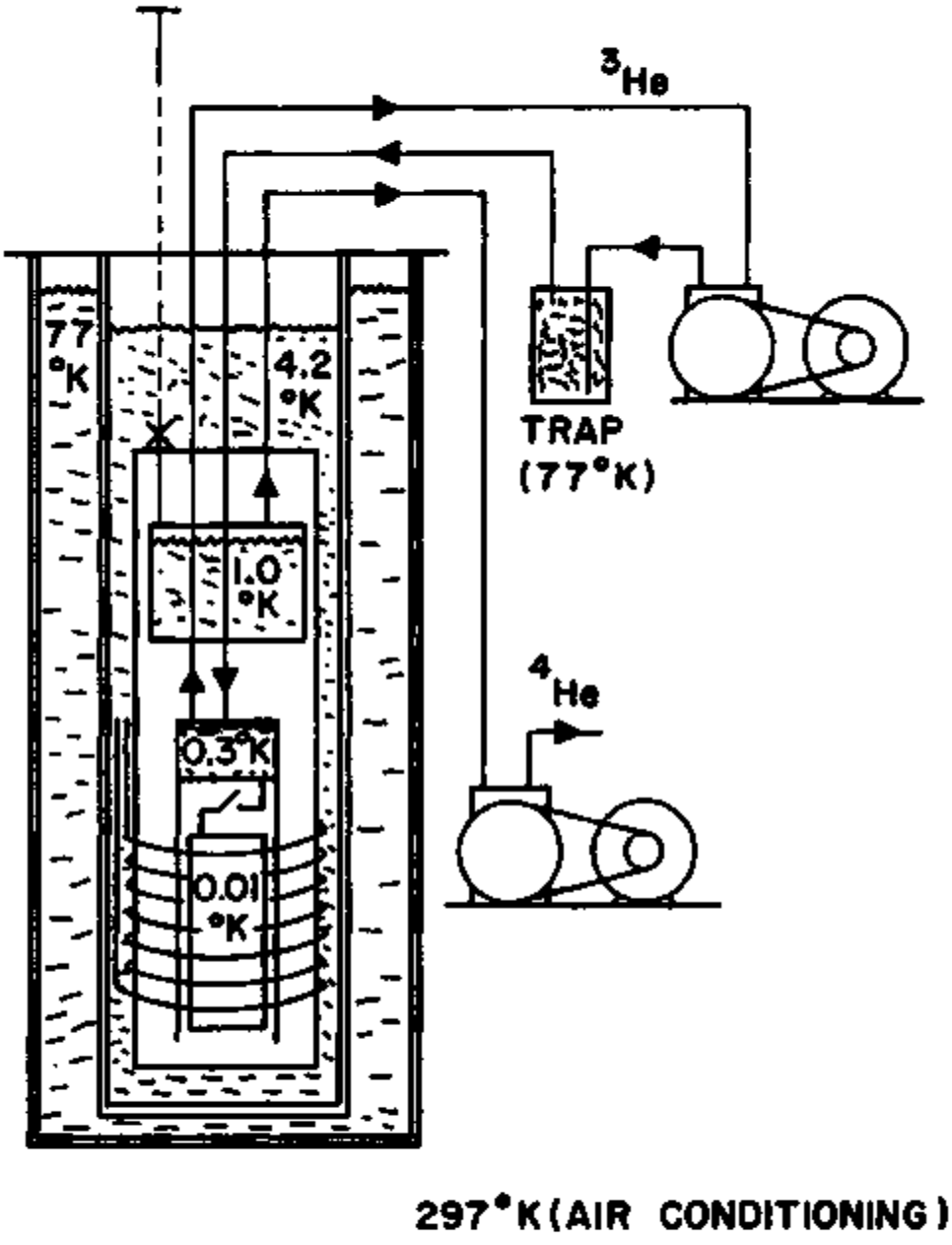

Figure 4. Block diagram of the apparatus.

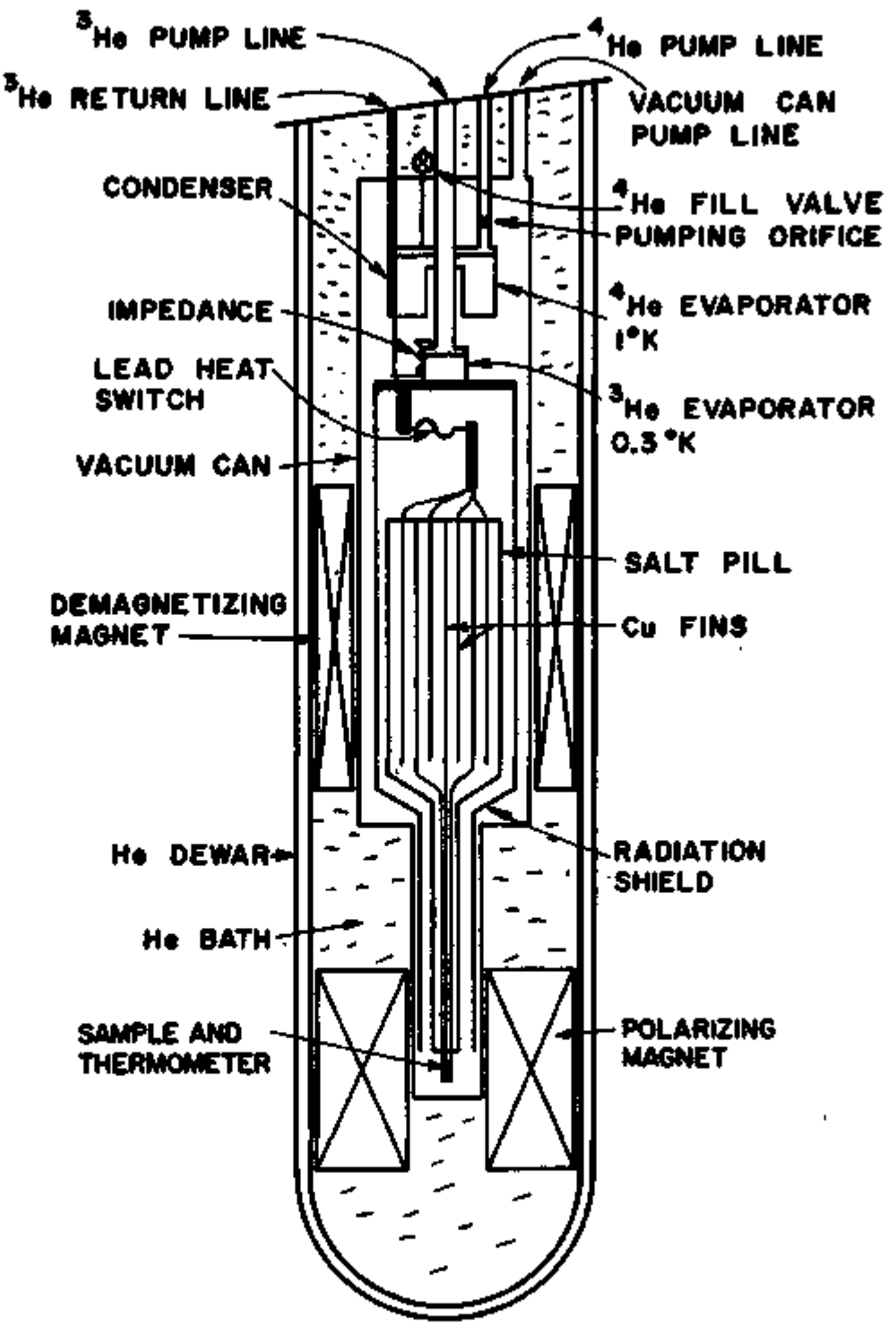

Figure 5. Schematic of the cryostat.

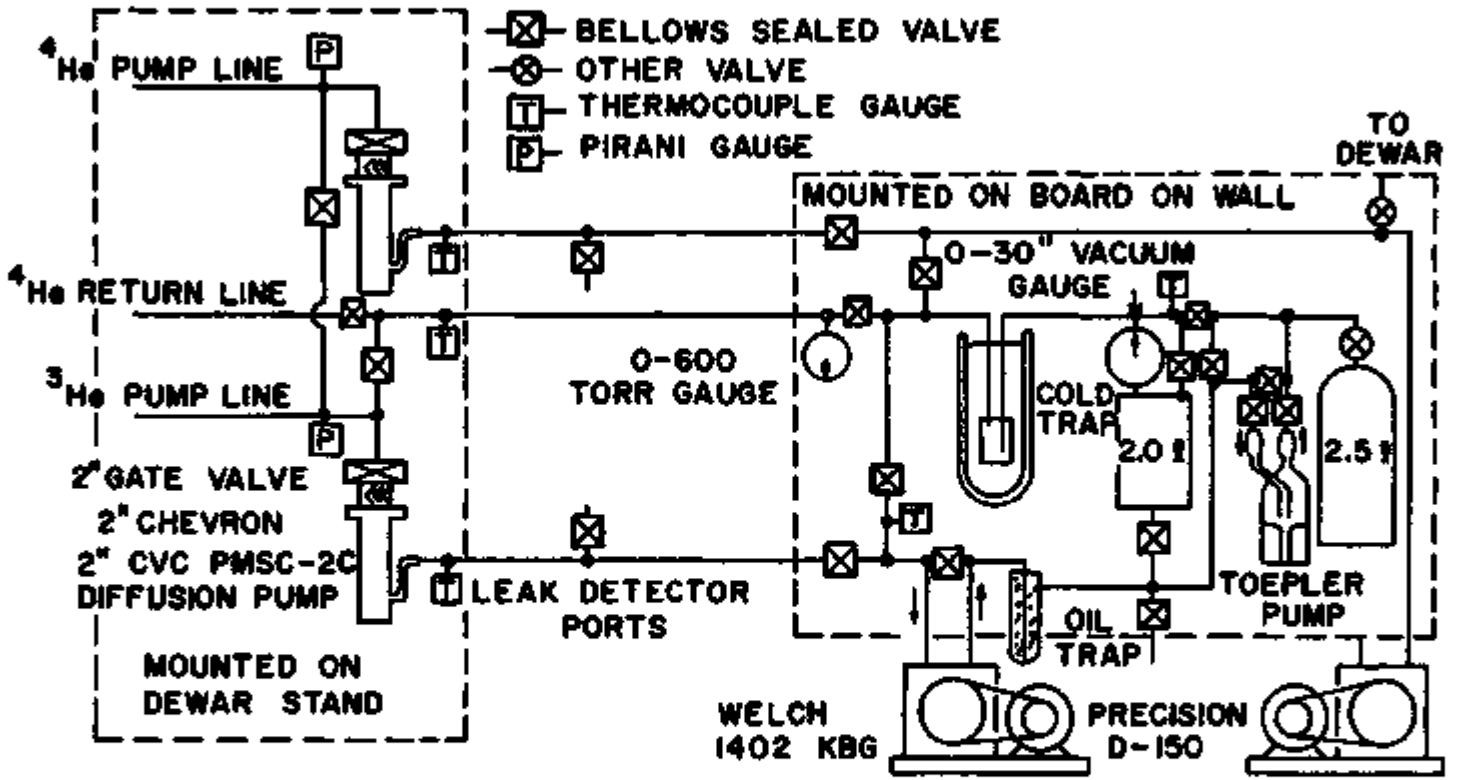

Figure 6. External gas handling system.

polarizing magnet was made by Magnion and has a 1-inch bore and is 6-inches in length. It was modified in order to fit into the helium dewar which has a 4-inch i.d. This magnet produces a maximum field of 40.7 kG at 17 amperes current. Both magnets are equipped with persistent current switches.

Inside the vacuum can are the ^{4}He and ^{3}He evaporators or pots. The ^{4}He pot, which has a volume of 77 cm^3, is filled by means of a needle valve which permits ^{4}He to enter the pot from the 4.2 K He bath. This valve is controlled from the top of the dewar stand. By pumping on the liquid in this pot it is possible to cool to 1.1 K.

Located beneath the ^{4}He pot is the ^{3}He pot which has a volume of 7 cm^3. This pot can be operated in the recirculation mode, i.e., ^{3}He is continuously returned to the pot. The condenser for the ^{3}He is wrapped around the ^{4}He pot. In the single-shot mode, i.e., ^{3}He is not returned, it is possible to cool to 0.3 K using a diffusion pump. Attached to this pot is a radiation shield which surrounds the salt pill assembly and stops any 4 K radiation from the vacuum can from reaching the salt pill. The salt pill assembly hangs from the ^{3}He pot by means of a graphite support rod and is thermally linked to the ^{3}He pot by means

of a pure lead heat switch with dimensions 0.4 x 2.5 x 0.013 cm. The lead heat switch is positioned so that when the demagnetizing magnet is run up the field is transverse to the lead which is then in its normal state and a good thermal conductor. However when the demagnetizing magnet is reduced slightly the lead switch goes superconducting and becomes a poor conductor, thereby thermally isolating the salt pill.

The salt pill assembly is made of several strips of 0.02 cm copper sheet inside a textolite tube. In the upper half of the salt pill assembly the copper sheets are separated so that the paramagnetic salt, in the form of a slurry, can be inserted between the copper fins. The copper fins linking the sample and cooling salt have a slurry contact area of ~900 cm^2. The salt pill holds ~300 ml of slurry. The copper fins extend an additional 12 inches beneath the slurry with the thermometer and sample attached to the end of the fins. The 12-inch extension is used so that the magnetic field at the salt pill due to the polarizing magnet is kept to a minimum.

The temperature of the main He bath, ^4He and ^3He evaporators, and salt pill before demagnetization are monitored by means of carbon resistor thermometers.

2. Gamma-Ray Detection System

This is shown schematically in Fig. 7. The lithium drifted germanium, Ge(Li), detector, preamp (model 1408C), amplifier (1416), and d.c. restorer (1414) were supplied by Canberra Industries. The d.c. restorer was not used in runs 37 and 43. A pileup rejector was not used due to the fact that a dead time error would have been introduced. It is possible to correct for the dead time thus introduced but this would have involved a modification to the pulse height analyzer. A typical γ-ray spectrum is shown in Fig. 8. Only 200 channels of the 400 channel pulse height analyzer were used to decrease data print out time on the teletype.

Even though the efficiency of the solid state detector was only 4% of that of a NaI scintillation counter, the increase in resolution obtained was felt to be the determining factor, especially since the effect to be measured was small and the background correction of utmost importance.

B. Thermometry

The temperature of the Co alloys was determined by observing W(0) for the 835 keV γ ray of ^{54}Mn dissolved in Cu. ^{54}Mn was chosen because the nuclear

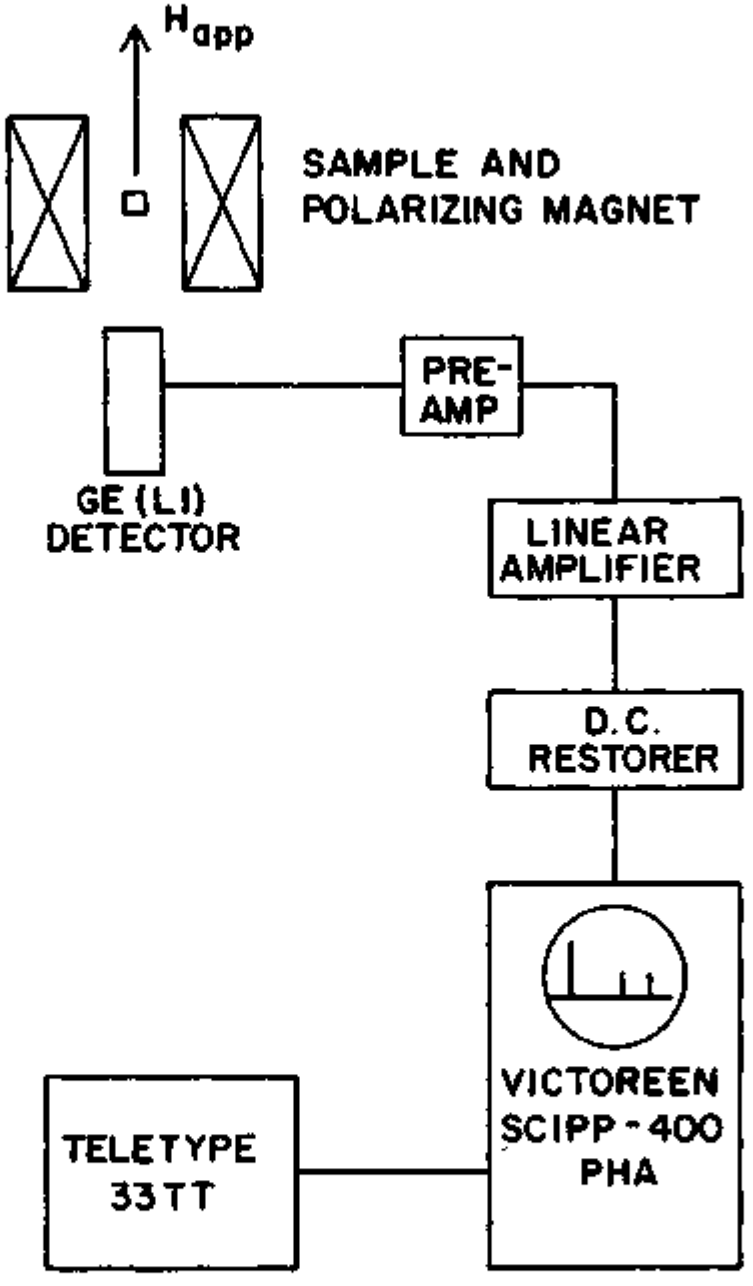

Figure 7. γ-ray detection and counting system.

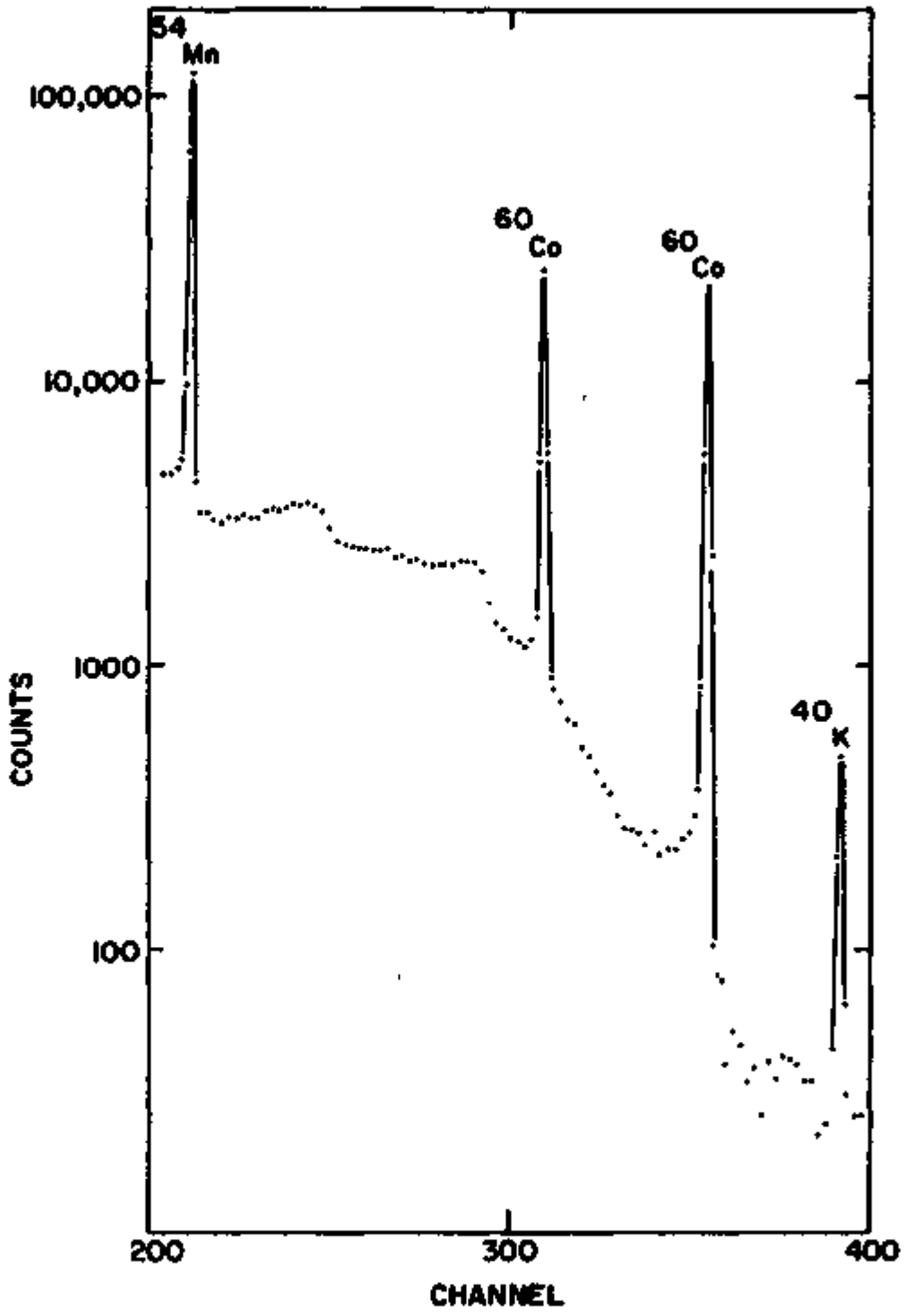

Figure 8. Typical one hour, warm γ-ray spectrum of the thermometer and sample. ^{40}K is part of the background.

parameters of interest are known. The decay scheme of ^{54}Mn is shown in Fig. 9. Also the 835 keV γ ray is lower in energy than the γ rays of ^{60}Co so that the Mn does not add any background to the ^{60}Co peaks. In addition ^{54}Mn decays by electron capture, therefore there is only a very small amount of heating as compared to that due to the emission of β particles.

The value of the internal magnetic field at the Mn nucleus for various applied fields has been determined previously.[15,21,22] Two of the three ^{54}Mn in Cu alloys used for thermometers were also calibrated against a ^{60}Co in Fe alloy. This will be discussed further in Chapter IV.

C. Sample Preparation

All alloys were prepared in a similar manner. Beginning with 0.013 cm sheets of 99.999% pure metal[23] (Au or Cu as required), ~0.8 cm^2 was cut off and then etched, (Cu in 1:1 HNO_3:H_2O and Au in hot aqua regia). For the alloys containing both Au and Cu the foils were etched and then trimmed to give the required weight ratio. $^{60}CoCl_2$,[24] specific activity 86.5 mCi/mg Co on 4/19/67, was evaporated onto the foils until the desired amount of activity was obtained. The foils were then placed in an alumina boat which was

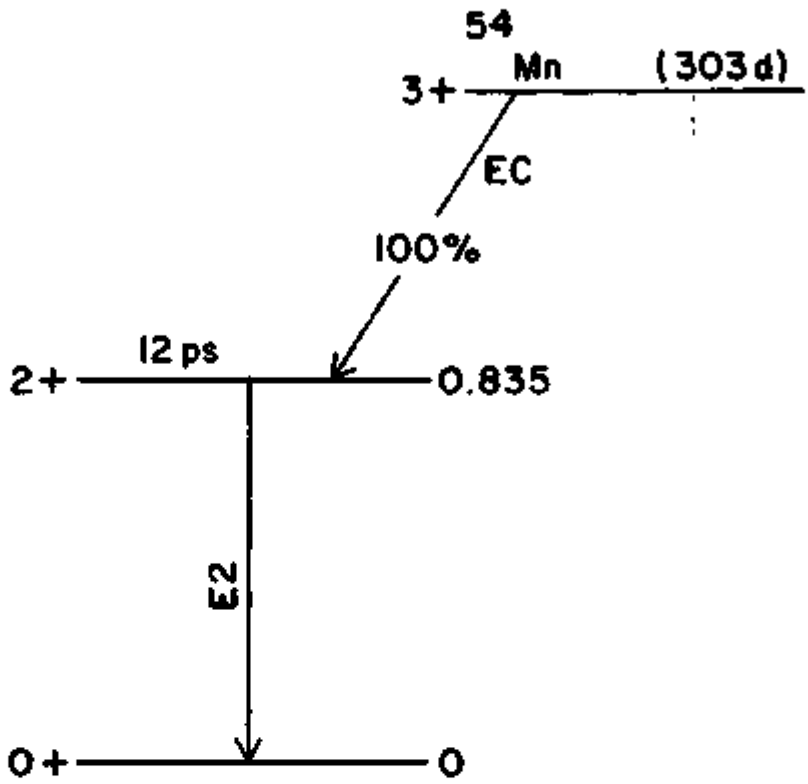

Figure 9. Decay scheme of ^{54}Mn.

inserted into a quartz tube. The tube was then flushed with gas. See Table I. Next the tube was slid into a resistance oven at 1100°C. The alloy was remelted several times by sliding the quartz tube in and out of the oven. The alloy was then removed from the oven and cooled (< ½ hour to reach room temperature) while still in the atmosphere given in Table I. When cool the alloy was etched in the appropriate acid and then flattened to 0.025-0.038 cm. The alloy was then annealed and cooled as in Table I.

All samples contained 5-7 μCi of ^{60}Co. Using the specific activity to calculate the concentration of Co in the alloys gives ~5 ppm Co. Resistivity ratio measurements were performed on both Au alloys giving $\rho(300\ K)/\rho(4.2\ K) = 190$ and 130. Taking 2.35 $\mu\Omega$-cm as the room temperature resistivity of pure gold and assuming a resistivity of 1 nΩ-cm/ppm for magnetic impurities,[12] the concentration of magnetic impurities is 12 and 18 ppm respectively.

D. Procedure

The alloy to be studied and thermometer were soldered with indium to the fins of the salt pill. Next the paramagnetic salt slurry was made up. For runs 37 and 43 cerium magnesium nitrate $[Ce_2Mg_2(NO_3)_{12}$

Table I. Sample preparation.

Run	Host	Atm. melted and annealed in	Annealing temp. (°C)	Annealing length (hrs)	Cooling after anneal
37	Au	5% H_2-95% Ar	650	16	slow[a]
43	Au	15% H_2-85% N_2	1000	2	fast[b]
49	Cu	5% H_2-95% Ar	750	6	"
50	Cu	"	750	18	"
51	Au_3Cu	"	800	12	"
52	AuCu	"	"	16	"
53	AuCu	"	"	18	"
55	AuCu	"	"	15	LN_2 quenched
58	$AuCu_3$	"	"	16	"

[a]sample cooled slowly to room temperature over a period of 8 hrs.

[b]sample cooled rapidly to room temperature over a period of ½ h.

$\cdot 24H_2O]$ was used. Chromium potassium alum $[CrK(SO_4)_2 \cdot 12H_2O]$ was used for all other runs. Crystals of cerium magnesium nitrate (CMN) were grown by using appropriate quantities of cerous nitrate and magnesium nitrate. These were then powdered with a mortar and pestle until able to pass through a No. 50 sieve. This powder was then mixed with glycerine until a slurry of the right consistency was obtained. The slurry was then packed between the fins of the salt pill. The chrome alum salt pills were made by powdering the alum as purchased.[25] Initially a mortar and pestle were used, however an industrial model Waring blender was found to do the job in much less time. The powdered chrome alum was mixed with equal volumes of glycerine and a saturated aqueous solution of chrome alum. A typical charge of slurry for the salt pill consisted of ~400 g of powdered chrome alum, 50 ml of glycerine, and 50 ml of saturated solution.

The salt pill was then suspended from the apparatus and the various leads and lead heat switch were soldered in place. Cd-Bi solder was used for the heat switch due to its good low temperature thermal conductivity.[26] Next the radiation shield was mounted in place. Thick cotton string around the bottom of the salt pill and heat shield served as thermal insulation

between pill, shield and vacuum can. An indium O-ring was used to insure a leak tight seal for the vacuum can. Then the superconducting magnets were mounted around the vacuum can. Finally both dewars were pulled up around the apparatus. The helium dewar was filled with dry nitrogen gas to insure cooling of the apparatus and the nitrogen dewar was filled with liquid nitrogen. The apparatus was then left overnight.

The following day the dry nitrogen was pumped from the inner dewar which was then filled with He gas. The vacuum can was pumped out and then filled to a pressure of ~1000 microns with H_2 gas. The H_2 served as an exchange gas. The liquid He transfer was then begun. This initial fill was always done slowly so that the innards of the apparatus would cool using the H_2 gas as a heat transfer medium. If the transfer was done too rapidly, the H_2 exchange gas would solidify and leave the apparatus at a high temperature. While filling with liquid He the magnets were run up and the ^{4}He pot filled and pumped on. Also ^{3}He gas was let into the ^{3}He pot. After ~4 hours the ^{3}He pot had cooled enough so that ^{3}He started to liquify. The ^{3}He pot was then pumped on in the recirculating mode. At this time 60 minute warm counts of the γ-ray

spectrum were started. After ~3 hours it was possible to stop recirculating the ^{3}He and go to the single-shot mode of operation with the ^{3}He diffusion pump on. After ~2 hours in this mode of operation the salt pill had cooled to 0.3 K and was ready to be demagnetized.

The demagnetization took 15 minutes and 5 minutes after completion of the demagnetization 60 minute cold counts were begun. Approximately 19 hours of cold counts were taken with a warm up rate of 1 mK every 5 hours. The salt pill was then remagnetized. The salt pill warmed up during remagnetization and warm counts were resumed. It took ~4 hours to cool the salt pill to the point where it was ready to demagnetize again. This cycle was repeated for a total of four demagnetizations, two with the polarizing field at one value and two with it at another. In this manner ~38 hours of cold counts were taken during each run for each value of the applied magnetic field.

IV. RESULTS

A. Treatment of Data

1. Background Correction

The total number of counts in each photopeak was determined by adding the counts in the appropriate channels. The background was accounted for by subtracting the counts in an equal number of channels lying immediately above the photopeak channels in energy. For example, if the photopeak fell in channels 330-337, then the background was taken as channels 338-345. The statistical error in this figure-number of counts in the photopeak, N, minus the background, B,-was given by $N-B\pm(N+B)^{\frac{1}{2}}$, where the error in N or B is the square root of the number.

After correcting for background, the two ^{60}Co peaks were added together. This can be done in this case due to the fact that the decay parameters of the ^{60}Co are such that $W(\theta)$ is the same for both γ rays.

2. Decay Correction

Since warm counts were taken over a period of several days and $W(0)$ was small, it was necessary to correct for the decay of the radioactivity. The warm counts were normalized back to the day of the first

warm counts by multiplying by $e^{\lambda t}$ where $\lambda = 0.693/t_{\frac{1}{2}}$ and t is the number of days elapsed between the first warm counts and the warm counts being corrected. $t_{\frac{1}{2}}$ is the half-life of the respective isotope. Next all warm counts were averaged. The error in the average of several counts is given by the error in one of the counts divided by the square root of the number of counts averaged.

The average of the warm counts was then corrected for decay to the day a sequence of cold counts was taken and this value was used in determining W(0), the cold count rate divided by the warm count rate. The percentage error in W(0) is given by $\pm(C^2+W^2)^{\frac{1}{2}}$ where C and W are the percentage errors in the cold count and warm count respectively.

No correction for solid angle was made as the Ge(Li) detector had a face surface area of 9.9 cm^2 and was located 20 cm from the source. For example, if W(0) for a one hour cold count had been 0.9600, the solid angle correction would have changed this to 0.9602. This difference is well within statistics and therefore negligible.

3. Least-Squares Fit

After W(0) for the ^{60}Co and 1/T as given by the ^{54}Mn thermometer were determined, the data was fed

into a computer and a least-squares fit to the theoretical expression for W(0) was performed to determine the value of the internal magnetic field, H_{int}, at the ^{60}Co nucleus. This was then plotted against the applied magnetic field, H_{app}, and a least-squares fit straight line was calculated.[27]

B. Co in Noble Metal Hosts

The results for all runs are summarized in Table II. The applied field values are known to better than ±3%. All other errors have been calculated assuming only statistical variations.

In Fig. 10 W(0) vs. 1/T for ^{60}Co in AuCu is shown. The data is typical of that obtained for the other hosts used. Each point in Fig. 10 is the average of several hour counts. In Fig. 11 H_{int} vs. H_{app} is plotted for Co in Au, AuCu, and Cu. The solid lines are least-squares fit to all the data whereas the dashed lines are fit only to the high H_{app} points and forced to go through zero. For the solid lines we have

$$H_{int}(kG) = (3.2\pm3.5)+(1.29\pm0.11)H_{app}(kG) \quad \text{(Au)}$$

$$H_{int} = (-2.6\pm2.8)+(1.28\pm0.08)H_{app} \quad \text{(AuCu)}$$

$$H_{int} = (5.7\pm3.9)+(0.92\pm0.12)H_{app} \quad \text{(Cu)}.$$

Table II. H_{int} *vs.* H_{app} for the ^{60}Co alloys.

Run	Host	H_{int}(kG)	H_{app}(kG)
37	Au	34.3(1.8)	24.0(0.6)
		51.3(0.7)	36.0(0.9)
43	Au	36.5(1.0)	25.5(0.7)
		43.1(0.8)	32.0(0.8)
		52.7(0.7)	38.9(1.0)
49	Cu	29.5(1.3)	28.7(0.7)
		43.5(1.3)	40.7(1.0)
50	Cu	32.2(1.0)	27.0(0.7)
		41.7(0.9)	38.9(1.0)
51	Au_3Cu	33.5(2.0)	27.0(0.7)
		48.0(2.0)	38.9(1.0)
52	AuCu	34.0(0.8)	27.0(0.7)
		47.5(0.8)	38.9(1.0)
53	AuCu	30.5(1.1)	28.7(0.7)
		50.0(0.8)	40.7(1.0)
55	AuCu	31.1(1.0)	26.4(0.7)
		45.3(0.8)	38.0(1.0)
58	$AuCu_3$	30.3(0.7)	28.7(0.7)
		45.4(0.7)	40.7(1.0)

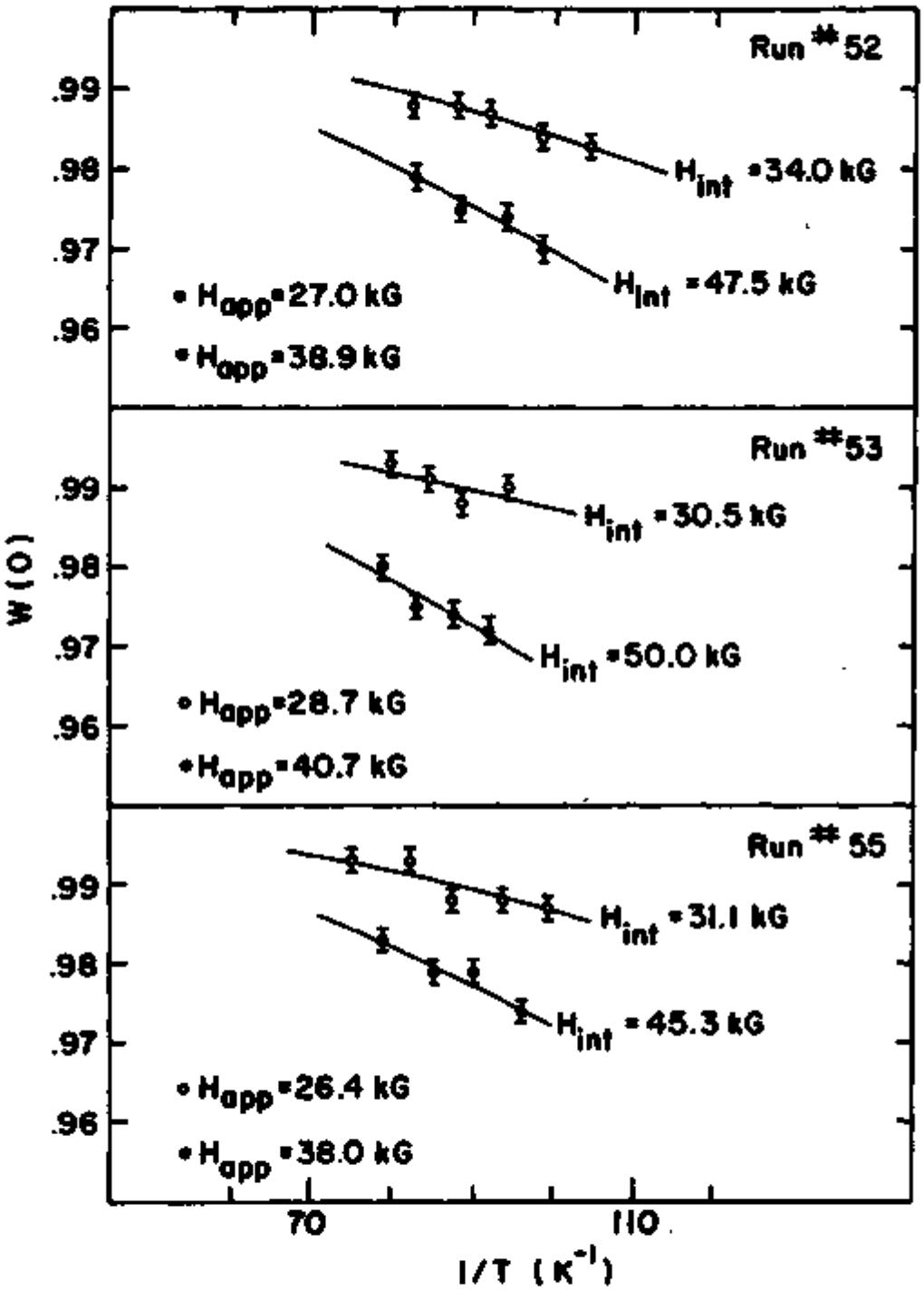

Figure 10. Gamma-ray anisotropy, W(0), of oriented ^{60}Co in AuCu as a function of reciprocal temperature for various values of H_{app} for three different samples. The curves are least-squares fits to the experimental data and were calculated using the values of H_{int} shown.

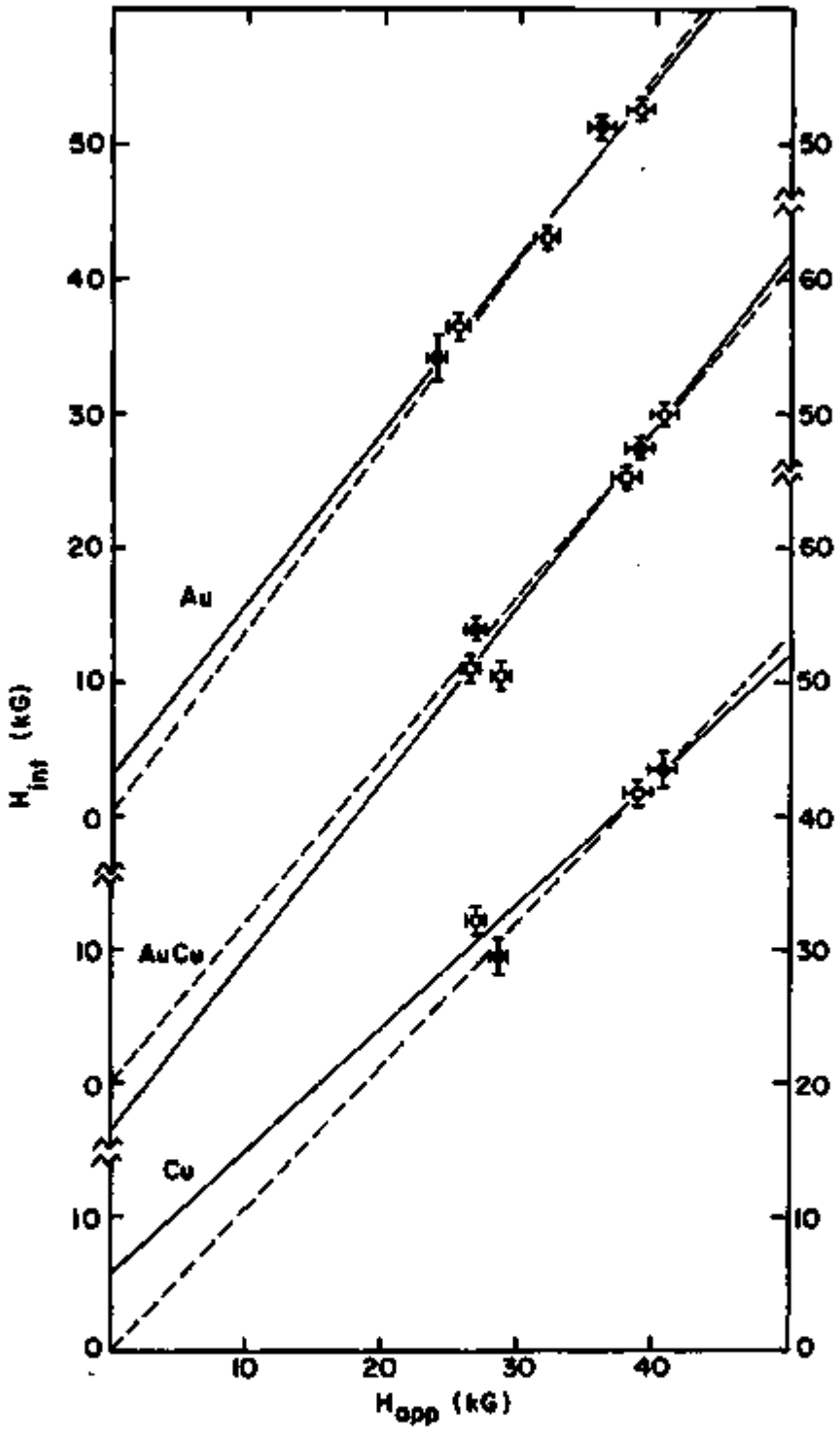

Figure 11. H_{int} vs. Happ for Au, AuCu, and Cu hosts. The solid lines are least-squares fit straight lines to all the data for a given host whereas the dashed lines are fit only to the high Happ points and are forced to go through zero at Happ = 0. Au host: o-run 43; •-run 37; AuCu host: o-run 53 •-run 52; □-run 55; Cu host: o-run 50; •-run 49.

The results for the Au and Cu hosts agree with the null results of Cameron et al.[28], who used a maximum applied field of 15 kG and 1/T of 70 K^{-1} at which the anisotropy for ^{60}Co in Au would have been only 0.3% and for ^{60}Co in Cu even less. The slopes of both the solid and dashed lines vs. host are shown in Fig. 12.

C. Calibration of Thermometers

Two of the three ^{54}Mn in Cu thermometers used were calibrated using a ^{60}Co in Fe source as the thermometer. The third thermometer was used only for the Co in Au_3Cu run. The results of these calibrations are shown in Fig. 13 along with the highest applied field points of Pratt et al.[22] and Campbell et al.[15] The statistical error in our data is less than the size of the points.

These thermometers were prepared in the same manner as the ^{60}Co alloys. They were annealed for several hours and then cooled to room temperature in less than ½ hour. Thermometer 2 was stored in liquid nitrogen until ready for use. It is possible that the discrepency shown in Fig. 13 between the two thermometers is due to the oxidation of the Mn in thermometer 1.[29] The concentration of Mn in the thermometers was less than 1 ppm.

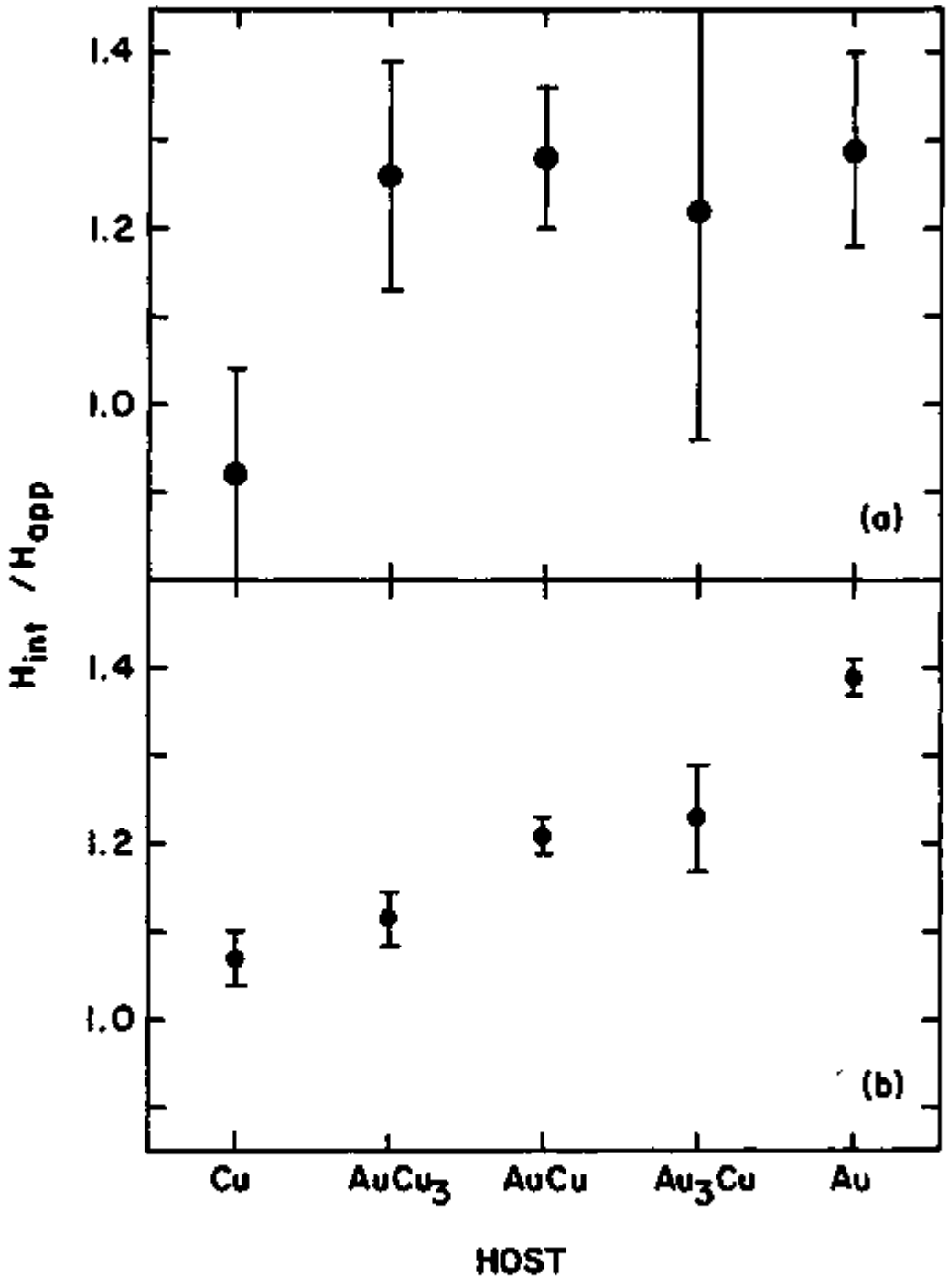

Figure 12. H_{int}/H_{app} vs. host. (a) All points have been used. (b) Only high H_{app} points have been used and H_{int} is set equal to zero at $H_{app} = 0$.

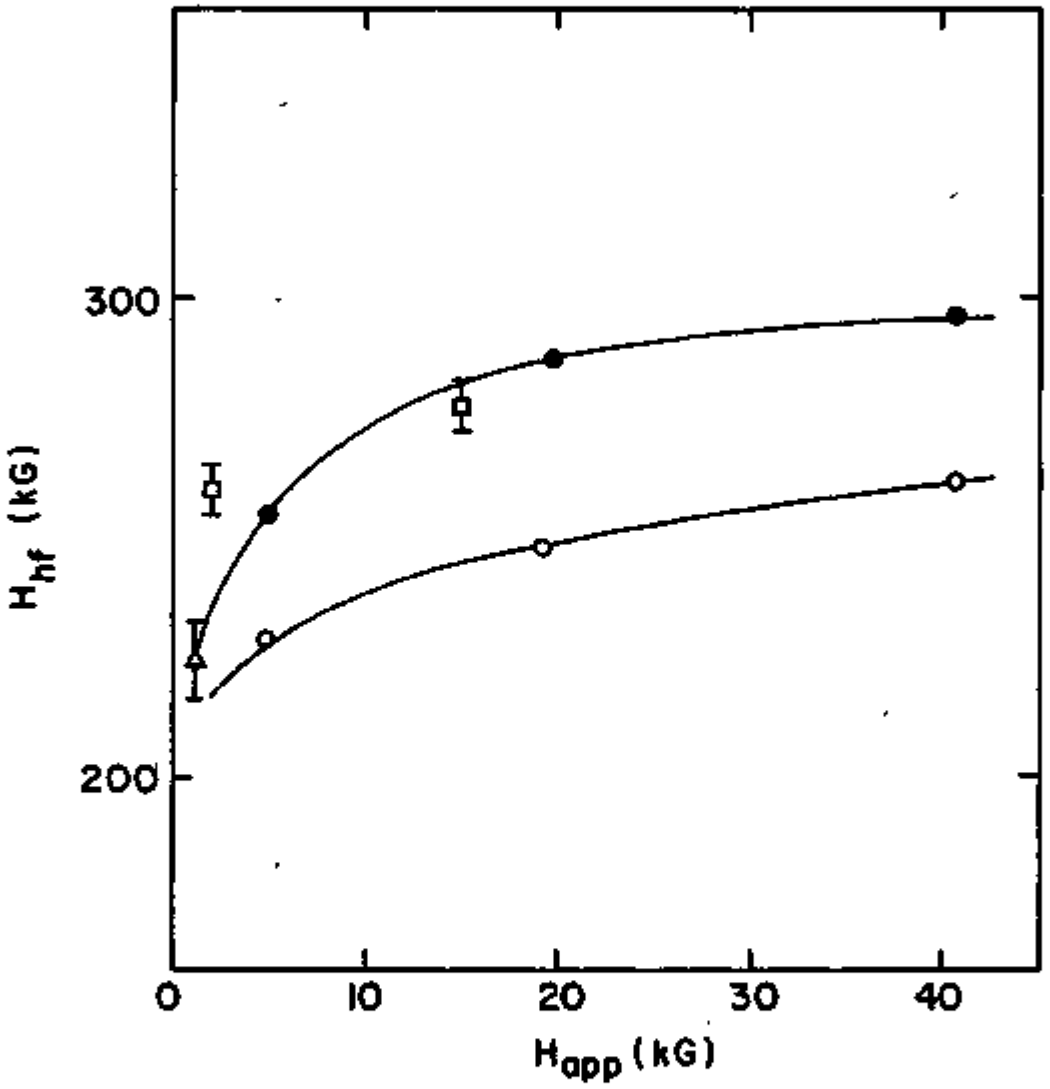

Figure 13. H_{hf} vs. H_{app} for ^{54}Mn in Cu thermometers. Open circles-thermometer 1; filled circles-thermometer 2; open squares- Ref. 15; open triangle-Ref. 22.

These orientation results extend to much higher values of $\mu H_{app}/kT_K$ than previous nuclear orientation[15] and Mossbauer[14] experimental points. Taking $T_K = 0.064$ K[24] for Mn in Cu, $\mu H_{app}/kT_K = 175$. Also they can be seen to verify the conclusion that the quasi-bound state does not break up completely until this ratio is very much greater than unity as mentioned in Chapter II, Section B.3.

Campbell et al.[15] obtain a value of 277±5 kG for the saturation hyperfine field at Mn nuclei in Cu. Our results show that the saturation field is at least 296±1 kG. This result agrees well with a value of 305 kG obtained from low temperature specific heat measurements on a Cu(Mn) sample in zero applied field.[30]

V. DISCUSSION

A. Co in Au

Two important features stand out in the plot of H_{int} vs. H_{app} for Co in Au. H_{int} is relatively large and extrapolates linearly to nearly zero at $H_{app} = 0$.

There are three alternative interpretations of these results. The first is that the hyperfine field is negative, i.e., $H_{int} = H_{app} - |H_{hf}|$, and Hildebrand's data[31] for the susceptibility and effective moment of 0.3% Co in Au is assumed correct for isolated cobalt impurities. Hildebrand found that the susceptibility followed a Curie-Weiss form,

$$\chi = N\mu^2/3k(T-\theta).$$

For the 0.3 at % Co in Au alloys, he found $\mu = 4.59\,\mu_B$ and $\theta = -247$ K. Letting $M/N_{T=0} = \mu_{eff}(0)$ with $M = \chi H$, we find that $\mu_{eff}(0) = \mu^2 H/3k\theta$. For H = 40 kG, $\mu_{eff}(0) = (7.4\times10^{-2})\mu_B$. Comparing this with the nuclear orientation result assuming a negative H_{hf}, we find $H_{hf}/\langle\mu\rangle$ = 95 kG/$7.4\times10^{-2}\mu_B$ or 1,280 kG/μ_B! This can be compared to 131 kG/μ_B for Co in Co metal[32] and 75±10 kG/μ_B for several transition metal impurities in noble metal hosts.[33] If Hildebrand's value of 4.59 μ_B is used for the saturation value, we find H_{sat} = 5,900 kG as compared to 225 kG in Co metal.[32]

H_{sat} is the saturation value of H_{hf} for very large values of H_{app}.

The second alternative explanation is that the hyperfine field is positive. If Hildebrand's data is used as before with H_{hf} = 15 kG for H_{app} = 40 kG, then $H_{hf}/\langle\mu\rangle$ = 207 kG/μ_B. The magnitude of this value is still somewhat large but certainly more reasonable than that of the previous explanation. However the positive sign of H_{hf} contradicts what is presently known about the hyperfine structure of the iron series elements. Co in the hosts Fe, Co, and Ni shows a negative hyperfine field.[34] The sign of the hyperfine coupling as measured for dilute alloys of transition metals in noble metal hosts is negative, e.g., Cr,[33] Mn,[28] and Fe[35] in Cu, Ag, and Au and V in Au.[2] For concentrations greater than 1.5 at % the V in Au hyperfine coupling becomes positive. This is thought to be due to V-V interaction effects. Cobalt in palladium apparently has a positive hyperfine coupling,[28] however this is a giant moment system.

The third interpretation of the results for Co in Au is that the hyperfine field is "normal" (say 130 kG/μ_B and negative) and μ_{eff} = 4.5 μ_B. Then the linear increase of magnetization with field is typical

of a Kondo type system with $T_K \sim 25$ K. In calculating T_K, the expression

$$\chi = (\mu_{eff})^2/3kT_K, \qquad T \ll T_K \qquad (3)$$

for the susceptibility was used, where μ_{eff} is the experimentally determined high temperature effective moment for the Co impurity. Daybell and Steyert have shown that at low applied fields, well below T_K, the magnetic susceptibility of the Cu(Fe) system is observed to follow Eq. (3).[39] In using Eq. (3) to calculate T_K, it was assumed that

$$H_{hf}/H_{sat} = M/M_{sat}$$

where $M = \chi H_{app}$ and M_{sat} is the saturation value of the impurity electronic moment: $M_{sat} = \mu_{eff}[S^2/S(S+1)]^{\frac{1}{2}}$. The final expression for T_K is

$$T_K = \mu_{eff}{}^2 H_{sat} H_{app}/3kM_{sat}H_{hf}. \qquad (4)$$

The value of μ_{eff} used is from Hildebrand's data for 0.3 at % Co in Au. If there are Co-Co interaction effects at this concentration, it is possible that μ_{eff} is larger than it would be for an isolated impurity. If μ_{eff} (and also H_{sat} and M_{sat}) were decreased by half, then $T_K \sim 25/2^2$ K = 6.2 K. If this is the case, then $\mu H_{app}/kT_K \sim 1.5$ for the largest

values of H_{app} used, indicating that evidence of magnetic saturation should be seen in the data. However larger values of H_{app} would be necessary in order to make any deduction about this matter.

Daybell and Steyert have determined from experimental data values of T_c, a characteristic temperature which forms an estimate of T_K.[1] For Co in Au they find T_c between 100 and 400 K. These values are determined from susceptibility, resistivity, specific heat, and thermoelectric power measurements. Thus it appears that this last explanation contradicts all previous work on Co in Au. However, if the Kondo temperature is indeed about 25 K, then most previous work has been done at concentrations somewhat too high, since the concentration should be somewhat less than 50 ppm times T_K.[36] The low concentration is necessary to insure the absence of impurity-impurity interaction effects.

Recent resistivity measurements on dilute (<0.1 at %) Co in Au alloys have given mixed results. The work of van den Berg et al.[37] showed virtually no low temperature minimum, while that of Loram et al.[38] showed a pronounced minimum at 13 K, though not of the familiar Fe in Cu form.[39] The difference between the susceptibility results ($T_K \sim 200$ K) and the

orientation data can be explained if the susceptibility can be written as

$$\chi_{total} = \chi_{local} + \chi_{nonlocal}. \qquad (5)$$

A nuclear orientation result would measure χ_{local} whereas a bulk susceptibility measurement would give χ_{total}. If χ_{local} and $\chi_{nonlocal}$ were of opposite sign, T_K as measured by bulk susceptibility experiments would be larger than that obtained by nuclear orientation. It is reasonable to assume that the two terms are of opposite sign if χ_{local} is due to the impurity moment and $\chi_{nonlocal}$ due to the conduction electrons attempting to cancel the moment. Golibersuch and Heeger have proposed that the susceptibility be divided as in Eq. (5) to explain their NMR results for Cu(Fe).[40] They suggest that the spin polarization around the partially magnetized impurity is oscillatory in form and extends over a long range. Narath and Gossard, however, do not observe the long range behavior in their NMR work on Au(V) alloys.[2]

It should be noted that Williams et al. have used nuclear orientation to measure T_K for Cr in noble metal hosts and find that their values agree with those of other types of experiments.[33] Also if the hyperfine field is taken as positive and Eq. (4)

used, $T_K \sim 200$ K for the same values of μ_{eff} and H_{sat} as used previously.

Regardless of the interpretation of the data used, it is clear that dilute Co in Au is magnetic at low temperatures in the presence of an applied magnetic field. The results to be discussed in Sections B and C of this chapter also have a bearing on the interpretation of the Co in Au results.

B. Co in Cu

The results for Co in Cu can also be interpreted in three ways. The first is that the hyperfine interaction for Co in noble metal alloys is negative and $H_{hf} \sim 0$ for Co in Cu. If this is the case, H_{int}/H_{app} should go to zero when $H_{hf} = H_{app}$, however the data of Fig. 12b shows a smooth change of H_{int}/H_{app} with host. This will be discussed further in the following section.

The second and third interpretations for Co in Cu are that the hyperfine field for Co in noble metal hosts is negative and $H_{hf} \sim 2H_{app}$ or the hyperfine field is positive and $H_{hf} \sim 0$. The data of Fig. 12b would support either of these explanations. However Heeger *et al.* have looked at the nuclear magnetic resonance of Cu containing 0.040 at % Co and found

no Knight shift for the Cu resonance to within ±0.2 G in applied magnetic fields up to 11 kG.[46] Since the Cu nuclei in the vicinity of a given Co atom are sensitive to the local conduction electron spin polarization caused by a local moment on the Co, the absence of a Knight shift and therefore a local moment tends to negate the possibility that $H_{hf} \sim 2H_{app}$.

No matter which interpretation is used it is clear that Co in Cu is nonmagnetic, i.e., the Knight shift is less than 10% at low temperatures in applied fields as large as 40 kG. This agrees with the recent work of Tournier and Blandin.[41] They propose, using susceptibility measurements, that it is necessary for the Co to be in a cluster of three or more before a magnetic moment is formed.

Transition element impurities are typically more magnetic in Au than in Cu. For example, Mn in Cu shows $T_K = 0.064 \pm 0.002$ K[22] while Mn in Au behaves like a free ion of spin 5/2 to below 0.020 K.[42] Similarly, the Kondo temperature for iron in copper is much higher than for iron in gold.[43] The Kondo temperature of a given element is typically lower in Au than in Cu. A possible explanation for this is that the value of the Fermi energy is 7.0 eV in copper and 5.5 eV

in gold.[44] The larger Fermi energy in copper indicates that it would take a greater energy splitting between spin up and spin down d electron states to move one spin state above the Fermi level and cause local moment formation. See Fig. 3.

C. Co in Au-Cu Alloys

The results for the Au-Cu alloys are given in Table II. The results as shown in Fig. 12a are surprising in that the value of H_{int}/H_{app} remains constant, within statistics, for hosts between Au and $AuCu_3$ and then there is a sudden decrease in going to Cu as the host. A possible cause for this type of behavior would be clustering of the gold and copper atoms. Since cobalt is more soluble in gold than copper, e.g., 15 at % as compared to 3 at % respectively at 900 °C,[45] the Co would be found mostly in the Au clusters causing the value of H_{int}/H_{app} to remain constant as long as there was a substantial amount of Au in the host. This explanation is difficult to believe as the $AuCu_3$ alloy and one of the AuCu alloys were quenched in liquid nitrogen after annealing thereby inhibiting the formation of clusters. Both of these alloys still give the large value of H_{int}/H_{app} and the quenched

AuCu alloy data agrees well with the rapidly cooled AuCu alloys. Also the fact that the intercept of the $H_{app} = 0$ point is positive for the Au and Cu hosts, negative for the $AuCu_3$ and AuCu hosts, and zero for the Au_3Cu host emphasizes the uncertainty in the low H_{app} points. The scatter in these points is greater than in the high H_{app} points, as is to be expected, since W(0) is smaller for low values of H_{app} and therefore any error, such as an incorrect background correction, will effect the low H_{app} points more than the high H_{app} points.

If the low H_{app} points are ignored and the $H_{app} = 0$ intercept required to pass through zero, see dashed lines in Fig. 11, the points in Fig. 12b are obtained. It is felt that this data, showing a gradual change from the magnetic behavior for Co in a gold host to the essentially nonmagnetic behavior in a copper host, more nearly represents the actual case as far as the relative comparison of hosts is concerned, since the Fermi energy changes smoothly from 5.5 to 7.0 eV in going from a Au host to a Cu host. Therefore, using the same explanation as in the previous section, as the Fermi energy increases it becomes more difficult for one of the d spin states to move above E_F and become partially or completely emptied thereby forming

a local moment. Then at temperatures below the Kondo temperature it requires larger values of H_{app} to break up the coupling between the conduction electrons and local moment, the smaller the high temperature local moment. Although this explanation is certainly crude, it cannot be denied that the value of E_F is of extreme importance in local moment systems.

VI. CONCLUSION

We have shown that at low temperatures for large values of applied magnetic field, Co as a dilute impurity in Au shows a surprisingly large Knight shift of 30%. This result is not consistent with previous measurements on this system or NMR measurements on V in Au, where the Knight shift is -1.5% in the dilute impurity limit. Co might be expected to behave somewhat like V, just as Cr and Fe are similar. The results for Co in Cu show, at very low temperatures in applied magnetic fields as high as 40 kG, a Knight shift of less than 10% indicating that the Co is nonmagnetic. The results for Co in a series of Au-Cu alloys indicate that the transition from the magnetic behavior in a gold host to the nonmagnetic behavior in a copper host occurs smoothly with the value of H_{int}/H_{app} decreasing from 1.3-1.4 in gold to essentially 1.0 for a copper host.

Considering all the data available, both from this thesis and other sources, one is led to two possible interpretations for the Co in noble metal system. One is that the hyperfine interaction is <u>negative</u> and H_{hf}/H_{app} varies smoothly from 2.3-2.4 in Au to ~2.0 in Cu. However the NMR results of Heeger <u>et al</u>. tend to negate this interpretation as discussed

in Chapter V, Section B. The second interpretation is that the hyperfine interaction is positive and H_{hf}/H_{app} varies smoothly from 0.3-0.4 in Au to~0 in Cu. The positive hyperfine interaction however is not in agreement with the several measurements on other transition metal impurities in noble metal hosts, all of which have a negative hyperfine field as discussed in Chapter V, Section A. The final resolution of this dilemma is dependent on further experiments.

ACKNOWLEDGMENTS

We would like to thank:

Mr. Robert Swinehart for his assistance in performing and analysing the data from some of the experiments described in this thesis;

The staff of the Physics Department for their excellent technical assistance;

One of us, R. J. Holliday, would particularly like to thank:

My wife, Marilyn, for her patience and encouragement;

The other members of the low temperature group for their friendship, especially Mr. Javed Aslam and Mr. Carl Smith with whom I have spent many hours discussing many things, even physics.

REFERENCES

1. M. D. Daybell and W. A. Steyert, Rev. Mod. Phys. 40, 380 (1968).

2. A. Narath and A. C. Gossard, Phys. Rev. 183, 391 (1969).

3. R. Tournier and A. Blandin, Phys. Rev. Letters 24, 397 (1970).

4. M. Bancroft, private communication.

5. R. J. Blin-Stoyle and M. A. Grace, Oriented Nuclei, in Handbuch der Physik, S. Flugge, Ed. (Springer-Verlag, Berlin, 1957) Vol. 42, p. 556.

6. S. R. de Groot, H. A. Tolhoek, and W. J. Huiskamp, Orientation of Nuclei at Low Temperatures, in Alpha-Beta-and Gamma-Ray Spectroscopy, K. Siegbahn, Ed. (North-Holland Publishing Co., Amsterdam, 1965), Vol. 2, p. 1199.

7. D. A. Shirley, Thermal Equilibrium Nuclear Orientation, in Annual Review of Nuclear Science, E. Segre, Ed. (Annual Reviews, Inc., Palo Alto, California, 1966), Vol. 16, p. 89.

8. C. D. Jeffries, Dynamic Nuclear Orientation (Interscience Publishers, New York, 1963).

9. For a discussion and review of local moments and the Kondo effect, see Refs. 1 and 12, and J. Kondo, Theory of Dilute Magnetic Alloys, in Solid State Physics, F. Seitz, D. Turnbull, and H. Ehrenreich, Eds. (Academic Press, New York, 1969), Vol. 23, p. 183.

10. J. Friedel, Suppl. Nuovo Cimento VII, 287 (1958).

11. P. W. Anderson, Phys. Rev. 124, 41 (1961).

12. A. J. Heeger, Localized Moments and Nonmoments in Metals: The Kondo Effect, in Solid State Physics, F. Seitz, D. Turnbull, and H. Ehrenreich, Eds. (Academic Press, New York, 1969), Vol. 23, p. 283.

13. J. Kondo, Progr. Theoret. Phys. (Kyoto) 32, 37 (1964); J. Kondo, Progr. Theoret. Phys. (Kyoto) 34, 204 (1965); J. Kondo, Progr. Theoret. Phys. (Kyoto) 36, 429 (1966).

14. R. B. Frankel, N. A. Blum, B. B. Schwarz, and D. J. Kim, Phys. Rev. Letters 18, 1051 (1967).

15. I. A. Campbell, J. P. Compton, I. R. Williams, and G. V. H. Wilson, Phys. Rev. Letters 19, 1319 (1967).

16. H. Ishii, Progr. Theoret. Phys. (Kyoto) 40, 201 (1968); S. M. Bose and T. Tanaka, J. Phys. C, 3, 958 (1970).

17. F. Takano and T. Ogawa, Progr. Theoret. Phys. (Kyoto) 35, 343 (1966); D. R. Hamann, Phys. Rev. 158, 570 (1967); Y. Nagaoka, Progr. Theoret. Phys. (Kyoto) 37, 13 (1967); H. Ishii and K. Yosida, Progr. Theoret. Phys. (Kyoto) 38, 61 (1967); A. P. Klein, Phys. Rev. 172, 520 (1968); J. Zittartz, Z. Physik 217, 155 (1968).

18. H. Suhl, Phys. Rev. Letters 19, 442 (1967); M. Levine and H. Suhl, Phys. Rev. 171, 567 (1968).

19. E. Fermi, Z. Physik 60, 320 (1930).

20. C. H. Smith and W. Weyhmann, Adiabatic Demagnetization Cryostat for Thermal Equilibrium Nuclear Orientation, AEC Report COO-1569-35.

21. J. P. Compton, I. R. Williams, and G. V. H. Wilson, in Hyperfine Structure and Nuclear Radiations, E. Matthias and D. A. Shirley, Eds. (North-Holland Publishing Co., Amsterdam, 1968), p. 793.

22. W. P. Pratt, Jr., R. I. Schermer, and W. A. Steyert, J. Low Temp. Phys. 1,469 (1969).

23. United Mineral & Chemical Corp., New York, N. Y.

24. Nuclear Science & Engineering Corp., Pittsburgh, Pa.

25. Mallinckrodt Chemical Works, St. Louis, Mo.

26. W. A. Steyert, Rev. Sci. Instr. 38, 964 (1967).

27. P. R. Bevington, Data Reduction and Error Analysis for the Physical Sciences (McGraw-Hill, Inc., New York, N. Y., 1969), Ch. 6.

28. Results from Clarendon Laboratory, Oxford, quoted by N. J. Stone in Hyperfine Interactions, A. J. Freeman and R. B. Frankel, Eds. (Academic Press, New York, 1967), p. 659.

29. D. H. Howling, Phys. Rev. 155, 642 (1967).

30. J. C. Ho, thesis, University of California, Berkeley, 1965 (unpublished), quoted in Ref. 15.

31. E. Hildebrand, Ann. Physik (5) 30, 593 (1937).

32. A. M. Portis and R. M. Lindquist, Nuclear Resonance in Ferromagnetic Materials, in Magnetism, G. T. Rado and H. Suhl, Eds. (Academic Press, New York, 1965), Vol. IIA, p. 369.

33. I. R. Williams, I. A. Campbell, C. J. Sanctuary, and G. V. H. Wilson, Solid State Commun. 8, 125 (1970).

34. D. A. Shirley, Table of Hyperfine Fields, in Hyperfine Structure and Nuclear Radiations, E. Matthias and D. A. Shirley, Eds. (John Wiley & Sons, Inc., New York, 1968), p. 979.

35. T. A. Kitchens, W. A. Steyert, and R. D. Taylor, Phys. Rev. 138A, 467 (1965).

36. M. D. Daybell and W. A. Steyert, J. Appl. Phys. 40, 1056 (1969).

37. G. J. van den Berg, J. van Herk, and B. Knook, Proc. 10th Intern. Conf. on Low Temp. Phys., Vol. IV, p. 272 (Vimitri Publishing House, Moscow, 1967).

38. J. W. Loram, P. J. Ford, and T. E. Whall, J. Phys. Chem. Solids 31, 763 (1970).

39. M. D. Daybell and W. A. Steyert, Phys. Rev. 167, 536 (1968).

40. D. C. Golibersuch and A. J. Heeger, Phys. Rev. 182, 584 (1969).

41. R. Tournier and A. Blandin, Phys. Rev. Letters 24, 379 (1970).

42. E. Lagendijk, L. Niessen, and W. J. Huiskamp, Phys. Letters 30A, 326 (1969).

43. J. W. Loram, T. E. Whall, and P. J. Ford, Phys. Rev. B, to be published.

44. C. Kittel, Introduction to Solid State Physics, 3rd ed. (John Wiley & Sons, Inc., New York, 1966), p. 208.

45. M. Hansen, Constitution of Binary Alloys, 2nd ed. (McGraw-Hill Book Co., Inc., New York, 1958).

46. A. J. Heeger, L. B. Welsh, M. A. Jensen, and G. Gladstone, Phys. Rev. 172, 302 (1968).